Composites Science and Technology 242 (2023) 110152

Contents lists available at ScienceDirect

Composites Science and Technology

journal homepage: www.elsevier.com/locate/compscitech

Sulfonated hypercrosslinked polymer enhanced structural composite supercapacitors

Olivier Hubert [a], Nikola Todorovic [a], Lina M. Rojas González [a], Elodie Costagliola [a], Alexander Blocher [a], Andreas Mautner [a], Robert T. Woodward [a,**], Alexander Bismarck [a,b,*]

[a] Polymer & Composite Engineering (PaCE) Group, Institute of Materials Chemistry and Research, Faculty of Chemistry, University of Vienna, Währinger Straße 42, 1090, Vienna, Austria

[b] Department of Chemical Engineering, Imperial College London, South Kensington Campus, SW7 2AZ, London, UK

ARTICLE INFO

Keywords:
Carbon fibers
Multifunctional composites
Porous polymer
Electro-chemical behaviour
Multifunctional properties
Structural supercapacitor

ABSTRACT

Structural supercapacitors are multifunctional devices able to bear mechanical load while storing electrical energy. Carbon fibres can be used as a bifunctional component within structural supercapacitors, acting both as current collector and mechanical reinforcement. A promising route to such devices is to increase the surface area of carbon fibres, which can be achieved by the deposition of active materials, and embed them into a structural electrolyte. A highly sulfonated, high porosity hypercrosslinked polymer was deposited onto carbon fibres by electrophoretic deposition from an aqueous suspension. We investigated the effect of polymer and binder concentration in the deposition suspension on the electrochemical properties of the coated carbon fibre electrodes. Multifunctional structural composite supercapacitors had a fibre volume fraction of only 21% and possessed a tensile strength and Young's modulus of 495 MPa and 49 GPa, respectively. A specific capacitance of 1.2 F/g was reached, comparable to graphene coated carbon fibre electrodes. At room temperature and ambient humidity an energy density of 39 mWh/kg and a power density of 15 W/kg were measured. We demonstrate that moisture plays a major role in the energy storage mechanism in these SCs.

1. Introduction

The development of multifunctional energy storage devices is being driven by electrification of all forms of transport. By consolidating both mechanical load bearing abilities and electrical energy storage into a single material, thus creating a multifunctional material, significant weight reductions in electric vehicles might be realised [1–3]. Carbon fibre-based structural energy storage devices include structural batteries [4], capacitors [5], and supercapacitors [6]. Batteries offer the highest energy density but limited power density due to their dependence on ion de/intercalation in the electrodes. Capacitors have high power density but low energy density due to reliance on physical interactions at electrode surfaces for the storage and release of energy. Supercapacitors (SCs) overcome the issue of limited surface area by addition of an electrolyte and formation of an electrical double-layer at the surface of each electrode; allowing energy storage within the electrochemical double layer, utilising the actual surface area of the electrode rather than the geometric surface, yielding both improved energy and power densities [7].

SC electrodes typically consist of a metallic current collector coated with high surface area carbon [8]. For structural applications, the role of the current collector is twofold, offering not only good electrical conductivity but also providing structural integrity to the device. A variety of carbonaceous materials potentially fulfilling these criteria was investigated as electrode/current collector materials, among which were commercially available activated carbon fibres, carbon nanotube papers, and carbon nanofoam sheets [6]. All of these carbons gave satisfactory electrochemical performance but did not offer sufficient mechanical properties. Over the past decade, the primary route adopted for structural SC electrode preparation has been the modification of polyacrylonitrile (PAN)-based carbon fibres. Carbon fibres were physically (heat treated) and/or chemically (using CO_2, HNO_3, oxidation in air, or KOH) modified to increase their surface area without deteriorating their mechanical properties [9]. These modifications, however,

* Corresponding author. Polymer & Composite Engineering (PaCE) Group, Institute of Materials Chemistry and Research, Faculty of Chemistry, University of Vienna, Währinger Straße 42, 1090, Vienna, Austria.
** Corresponding author.
E-mail addresses: Robert.woodward@univie.ac.at (R.T. Woodward), alexander.bismarck@univie.ac.at (A. Bismarck).

https://doi.org/10.1016/j.compscitech.2023.110152
Received 31 March 2023; Received in revised form 5 July 2023; Accepted 7 July 2023
Available online 10 July 2023

yielded only moderate specific surface area improvements, which did not result in sufficient increase of the specific capacitance when assembled into a SC. In other approaches, PAN-based carbon fibres were coated with high specific surface area carbon materials, such as carbon nanotubes [10], carbon aerogels [11,12], or graphene [13], coated via grafting, infusion, and spraying, respectively. The specific surface area was increased from around 0.3 m^2/g for pristine carbon fibres to above 180 m^2/g for graphene coated fibres. This increase in specific surface area translated to an improvement in specific capacitance from 0.1 F/g to 1.4 F/g of the assembled structural SC [10]. However, carbon nanotubes and graphene nanoplatelets are relatively expensive and coating carbon fibres with carbon aerogel is labour intensive and difficult to scale. Other examples include structural supercapacitors based on woven carbon fibre electrodes grafted with selenide-based nanowires [14] or continuous nanoporous networks [15]. Such devices were able to reach outstanding specific capacitances of up to 13.9 F/g while maintaining excellent mechanical properties. However, scalability of these devices has yet to be demonstrated. Additionally, structural pseudo-supercapacitors (systems that involve both electrostatic and electrochemical energy storage) have been investigated with promising performance [16].

One promising route to the scalable production of surface-decorated fibres is electrophoretic deposition (EPD). EPD is an easy, versatile, and scalable method to deposit materials onto a conductive substrate [17]. All charged colloidal particles able form stable suspensions can be used in electrophoretic deposition and, as such, many different battery or supercapacitor electrode materials have been EP deposited onto various substrates [18–20]. Recently, we showed that EPD can be used to produce graphene-decorated carbon fibres in a continuous process for use as supercapacitor electrodes [21]. EPD significantly broadens the amount of carbon fibre coatings that may be considered for energy storage, such as the use of synthetic polymers herein.

Hypercrosslinked polymers (HCPs) are a densely crosslinked subset of porous organic polymers with excellent chemical tunability [22]. The formation of HCPs utilises simple Friedel-Crafts chemistry, keeping costs low, and comprises “knitting” of aromatic compounds either with external crosslinkers or via self-condensation reactions. Hypercrosslinking requires only abundant Fe- or Al-based Lewis acids or even simple organic acids as polymerisation catalysts [23,24]. This feature allows broad HCP design options while requiring only mild reaction conditions and abundantly available reagents. Owing to their low costs, chemical versatility, and excellent thermal and chemical stability, HCPs are currently developed for many applications, such as separation and storage [25–27], and catalysis [28,29]. HCP networks were previously employed in energy storage applications either after carbonisation to improve electrical conductivity [30] or via hypercrosslinking of polymers with long range electron-pair conjugation [31].

We synthesised highly sulfonated HCPs (SHCPs) for subsequent electrophoretic deposition onto carbon fibres. HCP networks are typically non-soluble and hydrophobic, making electrophoretic deposition difficult. A high degree of sulfonation does significantly enhance network hydrophilicity, allowing for the formation of aqueous SHCP suspensions for electrophoretic deposition. SHCP coated carbon fibres are then assembled into supercapacitors in both liquid and structural electrolytes and their electrochemical and mechanical properties were characterised.

2. Experimental

2.1. Materials

1,2-Dichloroethane (≥99.0%), 4,4‘-bis(chloromethyl)-1,1‘-biphenyl (95%), and chlorosulfonic acid (99%) used for HCP synthesis were purchased from Sigma-Aldrich. Methanol (≥99.8%) was purchased from Fisher Scientific. Unsized, untreated polyacrylonitrile (PAN) based carbon fibres (12 k AS4D) were kindly provided by Hexcel. The binder, sodium carboxymethylcellulose (Na-CMC), was purchased from Sigma Aldrich. For the electrolytes, tetraethyl ammonium tetrafluoroborate ($TEABF_4$), propylene carbonate (PC), poly (ethylene glycol) diglycidyl ether (PEGDGE) and triethylenetetramine (TETA) were all purchased from Sigma Aldrich and 1-ethyl-3-methylimidazolium tetrafluoroborate (EMIM BF_4) from Iolitec. The separators were cellulose-based TF40-30 kindly provided by NKK Nippon Kodoshi Corp. For the preparation of structural SCs, absorbing paper (Whatman™ 520 A), release film (Upilex-25 S, UBE), and PTFE coated glass fibre peel-ply (FF03PM, Cytec Engineered Materials Ltd., UK) were used. The salts used to adjust the relative humidity were NaBr, purchased from Sigma-Aldrich, and KCl bought from VWR International. All materials were used as received.

2.2. Synthesis of sulfonated hypercrosslinked polymers

SHCPs were produced in a one-pot reaction following our previous report [32]. 4,4‘-Bis(chloromethyl)-1,1‘-biphenyl (2 mmol, 0.502 g) was first dissolved in 1,2-dichloroethane (DCE, 5 mL) at room temperature and stirred for 10 min at ~150 rpm. Subsequently, the solution was cooled to ~0 °C using an ice bath and stirred again for a period of 10 min. The speed was then increased to ~250 rpm and a solution of chlorosulfonic acid (4 mmol, 0.532 mL) in DCE (1 mL) was added. After 15 min, a reflux condenser was attached to the reaction and the solution was heated to 80 °C for 22 h. After heating, the resulting brown/black solid was washed with ~50 mL of methanol using a Büchner funnel. Finally, to remove excess methanol, the polymer was air dried before drying in a vacuum oven at 60 °C overnight. The polymer powders were dark brown to black and were typically produced in yields of >90%.

2.3. Electrophoretic deposition of SHCPs onto carbon fibres

Aqueous suspensions of SHCPs were prepared by first ball milling the polymer for 5 min before dispersing it in water (350 mL). Polymer suspensions with concentrations 0.8, 1.1, 1.6, 3, and 4 g/L were investigated. Na-CMC in concentrations of 0.45, 1.6 or 2.25 g/L was added to the aqueous suspension as binder to improve SHCP adhesion to the carbon fibres. The used electrophoretic deposition setup was described previously [21]. Briefly, the carbon fibres were attached to a purpose-built 3D-printed polylactic acid (PLA) holder and immersed in the SHCP aqueous suspension. Four interconnected immersed graphite paper sheets of 4 × 5 cm^2 acted as counter electrode (Fig. 1a). All depositions were performed using 20 V provided by a laboratory power generator (EA-PS 3065-05 B, Elektro-Automatik) for 150 s. After deposition, the fibres were removed from the suspension and pre-dried with a heat gun before drying in a vacuum oven at 60 °C for 2 h under reduced pressure. After coating, the part of the carbon fibre wrapped around the holder was removed as the contact did not allow for homogeneous deposition. The resulting SHCP coated carbon fibres were then used as electrode for SC assembly. A few cm of uncoated carbon fibres was left on each electrode for ease of connection to the potentiostat (Fig. 1b).

2.4. Characterisation of sulfonated hypercrosslinked polymers

N_2 adsorption isotherms of SHCPs were measured (Tristar II Plus, Micromeritics) at −196 °C on as prepared networks, networks after ball milling, and SHCP coated carbon fibres. Surface areas were determined using the Brunauer-Emmet-Teller (BET) method on the adsorption branch of the isotherm in the relative pressure (P/P_0) range of 0.05–0.2. Total pore volume V_T was determined from the total volume of N_2 adsorbed at P/P_0 = ~0.97 and micropore volume V_μ was calculated using the t-plot method in the P/P_0 range 0.15–0.4. For materials exhibiting low specific surface area, A_s, below the analytical threshold of volumetric nitrogen adsorption, e.g. for pristine carbon fibres, inverse gas chromatography (iGC) was employed at 70 °C and 0% RH using a surface energy analyser (Surface Measurement Systems). (Coated) Carbon fibres or polymer powder were inserted into a measurement column

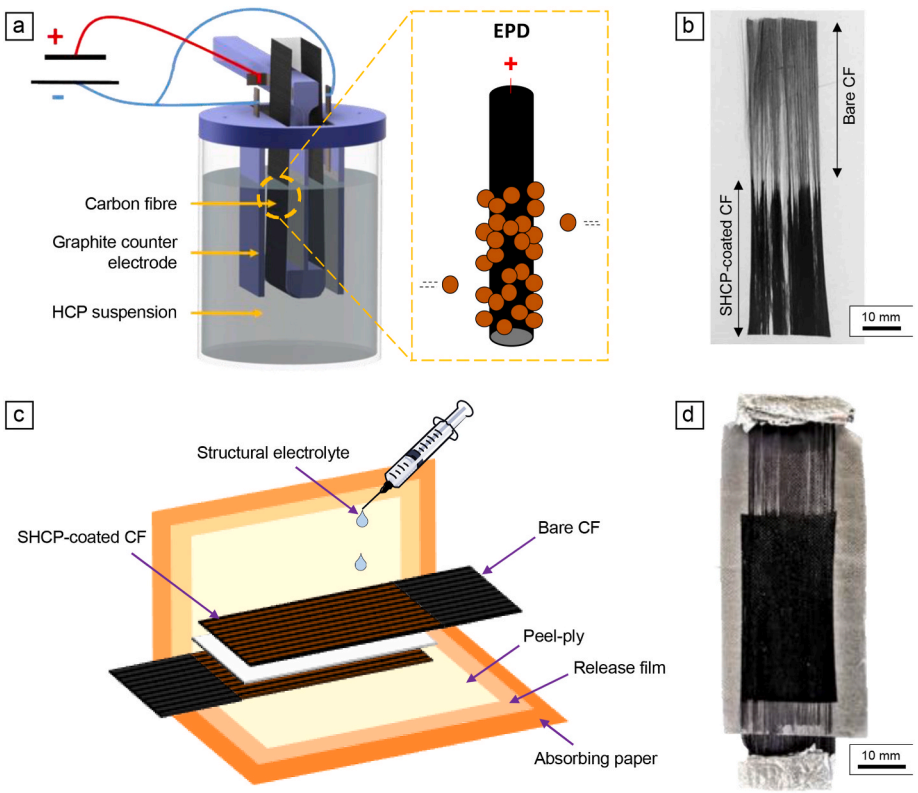

Fig. 1. A) Schematic of the EPD setup. b) Photograph of SHCP coated carbon fibre electrodes. SHCP coated carbon fibres appear black on the picture and uncoated fibres grey. c) Schematic layup of structural SC impregnation. d) Photograph of a structural SC with Al foil added for electrical connection.

(inner diameter 4 mm). A_s of the samples was then determined by octane retention at various coverages and P/P_0, and computed using the BET model from the centre of mass of the peaks. Fourier-transform infrared spectroscopy (Tensor II FT-IR Spectrometer, Bruker) was performed on finely ground samples in the range 4000–350 cm^{-1}. Elemental analysis (Eurovector EA 3000 CHNS–O Elemental Analyser) was performed on 0.75–3.0 mg of each sample, weighed into tin vials (4 × 6 mm) for each individual run. Each sample was ran at least in duplicate. Solid-state NMR (Avance NEO 500 wide bore system, Bruker BioSpin) was measured using a 4 mm triple resonance magic angle spinning (MAS) probe. Between 15 and 25 mg of material was packed into a 4 mm zirconia CRAMPS rotor. The resonance frequency for ^{13}C NMR was 125.78 MHz, the MAS rotor spinning was set to 14 kHz. Cross polarisation was achieved by a ramped contact pulse with a contact time of 3 ms. During acquisition ^{1}H was high power decoupled using SPINAL with 64 phase permutations. The ^{1}H $\pi/2$ pulse was 2.5 μs, the relaxation delay was set to 4 s, and with roughly 2000 scans a sufficient signal to noise ratio was achieved. The morphology of the SHCP coating on the carbon fibres was analysed by scanning electron microscopy (Zeiss Supra 55 V P, Zeiss). The amount of coating $C_{\%}$ on the carbon fibres was evaluated by gravimetric analysis using Eq. (1):

$$C_{\%} = \frac{m_t - l_t \cdot \lambda}{m_t - l_{nc} \cdot \lambda} \bullet 100 \qquad \text{Eq. 1}$$

where λ is the carbon fibre tow linear density (λ = 0.765 g/m), m_t the total mass of the specimen {coated carbon fibres + non-coated carbon fibres}, l_t the total length and l_{nc} the length of non-coated carbon fibres (Fig. 1b). The electrode mass m_e was calculated by adding $C_{\%}$ to the carbon fibre weight ($m_{CF} = (l_t - l_{nc}) \bullet \lambda$).

2.5. Supercapacitor assembly

Supercapacitors were assembled either with a liquid electrolyte or a structural electrolyte. In the text SC will refer to supercapacitors containing a liquid electrolyte and structural SC to supercapacitors containing a structural electrolyte. The electrolytes, as well as the assembly procedure, were described previously [21]. Briefly, for devices containing liquid electrolyte, two electrodes were superimposed with a separator layer in between and impregnated with 1 mL of electrolyte (1 M $TEABF_4$ in PC) by drop casting. For the liquid electrolyte, the SC assembly was performed in a 3D-printed PLA frame that ensured good contact between the layers when testing.

The assembly of structural SCs was performed in a glovebox (MBraun) under Ar atmosphere. The structural electrolyte was prepared by mixing PEGDGE (82.6 wt%), TETA (7.4 wt%) and EMIM BF_4 (10 wt %). The resulting mixture (0.7 mL) was drop casted onto the SC layup. The SC layup was placed between – from outside to inside – an absorbing paper to absorb any excess electrolyte, a release film to avoid adhesion of the SC to the absorbing paper, and a PTFE coated glass fibre peel-ply to aid electrolyte distribution in the fibre assembly (Fig. 1c). The layup was then pressed between two steel plates using spring clamps and placed into the oven compartment of the glovebox. The structural electrolyte was cured for 2 h at 80 °C under reduced pressure. After curing, the devices were taken out of the glovebox and Al foil was folded around the uncoated part of the carbon fibres to connect the testing device (Fig. 1d).

2.6. Supercapacitor characterisation

All electrochemical measurements were carried out using a potentiostat (Reference 600, Gamry instruments or BT-2043, Arbin Instruments). The SCs were tested with cyclic voltammetry (CV) between −1 V and 1 V at a rate of 5 mV/s for three cycles, unless stated otherwise. The capacitance was calculated at an applied difference of potential U = 0 V during the second and the third cycle for both increasing and decreasing voltage. Capacitance for SCs was the average of four values

calculated using Eq. (2),

$$I = C \bullet \left(\frac{dU}{dt}\right)_{U=0} \quad \text{Eq. 2}$$

where I is the measured current, U the applied difference of potential between the two electrodes and C the capacitance. The data sampling size for capacity determined for SCs produced from various EPD suspension concentrations used for Student's t-test were as follows: 7 samples for 0.8 g/L, 7 samples for 1.1 g/L, 11 samples for 1.6 g/L, 14 samples for 3 g/L, and 9 samples for 4 g/L. To assess long term performance of the assembled structural SCs, CV was measured with various boundaries and scan rates. These included boundaries of −4 V to 4 V, −1 V to 1 V, and −0.5 V to 0.5 V, all at a scan rate of 50 mV/s, as well as −1 V to 1 V at a scan rate of 5, 20, 50, and 100 mV/s. Coulombic efficiency was calculated from charge-discharge curves with a current density of 0.4 mA/g. Rate dependent charge-discharge was investigated by measuring discharge currents of 0.5, 0.8, 1, and 2 mA/g.

The equivalent series resistance (ESR) was estimated by electrochemical impedance spectroscopy (EIS) with frequencies ranging from 1 MHz to 0.1 Hz [33]. The EIS was measured using an AC voltage of 10 mV rms with respect to open circuit voltage (OCV). The energy density E and the power density P were calculated using Eq. (3) and Eq. (4), respectively,

$$E = \frac{1}{2}\, C_s \bullet U^2 \quad \text{Eq. 3}$$

$$P = \frac{U^2}{4 \bullet ESR} \quad \text{Eq. 4}$$

where C_s ($= \frac{C}{m_e}$) is the specific capacitance and U the applied voltage.

The impact of relative humidity (RH) on the electrochemical performance of structural SCs was assessed by CV between −0.5 V and 0.5 V at a rate of 20 mV/s, and EIS. For RH = 0%, the supercapacitors were placed in a pouch cell in a glovebox and tested therein. RH = 35% was the ambient RH in the laboratory at the time of measurement. For measurements at RH = 58 and 84%, the structural SCs were placed in a desiccator containing saturated salt solutions of either NaBr or KCl, respectively. The devices were equilibrated at the desired RH overnight and tested in the desiccator. All measurements were done at room temperature (between 23.5 and 24.5 °C). Five structural SCs were tested at each condition.

For mechanical testing, SHCP coated carbon fibres were cut into 210 mm long strips. The average width of the individual electrode strips was 25 mm. A total of 8 electrodes per specimen were used to manufacture multi-layered structural SCs. A separator layer was placed between each electrode layer. Five samples were manufactured simultaneously. A vacuum bag was prepared on an aluminium plate and the prepared fibre electrodes were placed into the bag. The layup consisted of a layer of polyimide release film on the Al plate, a layer of PTFE coated glass fibre peel-ply (FF03PM, Cytec Engineered Materials Ltd.), five specimens, another layer of peel-ply followed by release film and finally the vacuum bag. A strip of separator was placed on top of each electrode layer and drop casted with 0.6 mL structural electrolyte. This process was repeated until a thickness of 8 electrode layers was obtained, leaving the outermost layer as electrodes. The vacuum bag was then sealed with thermal resistant tape (Airdam 1, Airtech) and a 21 × 21 cm^2 metal plate with a thickness of 1 cm was placed on top. The vacuum bag was then press-claved. Vacuum was applied and the temperature of the hot press raised to 80 °C. A pressure of 0.75 MPa per sample was applied. After 10 min, the vacuum pump was turned off. To ensure complete curing, the specimens were hot pressed for 24 h at 80 °C.

The tensile properties of structural SCs as well as monofunctional carbon fibre reinforced structural electrolyte composites were measured adapting ASTM D3039. Samples were cut to a width of 25 mm. Glass fibre epoxy composite end tabs of 40 × 25 mm^2 were attached either side of the specimens using Araldite® glue. The remaining gauge length was 140 mm and composite thickness varied between 0.52 mm and 0.63 mm. The prepared specimens were loaded in tension using a universal test frame (Dual Column Universal Test System, Model 5969, Instron) equipped with a 50 kN load cell and a non-contact video extensometer (Gig ProE, iMETRIUM) at a loading rate of 1 mm/min. The ultimate tensile strength was calculated from the maxium load and cross-sectional area of the specimen. Young's modulus was determined from the linear elastic region of the stress-strain curve as secant between stresses separated by 0.25% strain. Average mechanical properties were derived from 5 tested samples.

3. Results and discussion

3.1. Sulfonated hypercrosslinked polymer

We confirmed successful SHCP formation using ^{13}C cross-polarisation/magic angle spinning solid-state NMR (CP/MAS ssNMR) (Fig. S1). The signal at ~38 ppm is assigned to crosslinking methylene bridges. The signal at ~120 ppm in the shoulder of a larger peak is assigned to the *C*–S bond formed during sulfonation. Signals at ~129 and ~139 ppm are assigned to aromatic (C_{Ar}-H) and quaternary, or substituted, aromatic carbons (C_{Ar}-R), respectively. We also confirmed successful polymer formation and sulfonation using FT-IR (Fig. S2). There, bands assigned to aromatic carbon, –SO_3H, and *C*–S bonds were observed. We employed CHNS–O elemental analysis (EA) to charaterise the bulk chemical composition of the network, which gave values of 56.9 wt% C, 4.5 wt% H, <0.5 wt% N, 11.3 wt% S and 24.7 wt% O. The presence of high amounts of sulfur confirm successful sulfonation, equating to a –SO_3H concentration of 3.5 mmol g^{-1}.

The SHCP's N_2 adsorption isotherms displayed characteristics of both Type I and Type IVa (Fig. S3), with adsorption at low relative pressures signalling microporosity and hysteresis deriving from capillary condensation in mesopores. The total pore volume and micropore volume were 0.38 ± 0.02 cm^3/g and 0.19 ± 0.01 cm^3/g, respectively, confirming a broad pore size distribution. The BET specific surface area, A_s, was 715 ± 32 m^2/g, in line with our previous report [32].

3.2. Sulfonated hypercrosslinked polymer decorated carbon fibres

After ball milling, SHCP was deposited onto carbon fibres from a 3 g/L suspension containing Na-CMC at a concentration of 0.45 g/L. Using SEM, we observed relatively low coverage of the fibre surfaces after SHCP deposition (Fig. 2a and b). For comparison, SEM images of bare fibres prior to deposition are also provided (Fig. S4). Low SHCP loading on the carbon fibres was confirmed by gravimetric analysis; the coating density was 9.6 ± 2.5 wt%, which equates to 82 ± 23 mg of SHCP/m of carbon fibre tow. The morphology of the deposited SHCP was in line with previous HCP examples [29,34], appearing as agglomerates of SHCP particles of <100 nm in diameter (Fig. 2c and d).

After ball milling, A_s of the SHCP was reduced to 460 ± 40 m^2/g. The N_2 adsorption isotherm of ball milled polymer is compared to the as prepared polymer in Fig. S3. The reduction in surface area associated with ball milling was predominantly assigned to the destruction of micropores, as shown by a reduction in V_μ from 0.19 cm^3/g to 0.13 cm^3/g (V_T decreased from 0.36 cm^3/g to 0.27 cm^3/g). Using the surface area value after milling and the coating weight, A_s of the carbon fibres after SHCP deposition was estimated to be 45 ± 12 m^2/g. However, the A_s we obtained from N_2 adsorption isotherms was merely 8.9 ± 2.6 m^2/g, which corresponds to a SHCP loading on the carbon fibres of around 1.9 wt%. This difference is likely due to a combination of factors, including the deposition of some binder as coating, which does not contribute to surface area increase, and inaccuracies in the measurement caused by relatively low surface areas. To further investigate the variation of A_s and calculate the amount of SHCP attached, taking into the account the A_s of carbon fibres, we measured A_s using iGC, which allows for

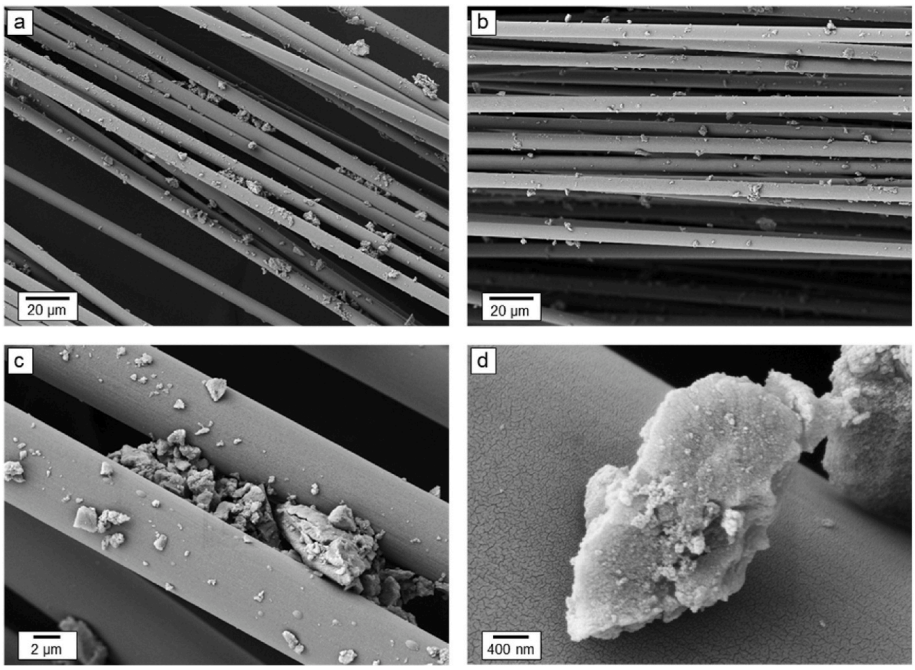

Fig. 2. Characteristic micrographs of carbon fibres after SHCP deposition. (a) and (b) 500× magnification, (c) 3000× magnification, and (d) 20,000× magnification.

characterisation of low A_s materials, i.e. carbon fibres. The A_s determined from iGC peak maxima of SHCP and SHCP coated carbon fibres was 49.4 m^2/g and 1.7 m^2/g, respectively. The A_s values obtained from iGC varied substantially from those obtained from N_2 adsorption isotherms due to differences in measurement temperatures and probe molecule. Moreover, for the first figure (9.6 wt%) a balance was used to determine the weight, where the contribution of binder and SHCP cannot be differentiated. The following values (1.9 and 3.3 wt%) were determined by BET and iGC, respectively. Therein the binder will have negligible impact as it has no measurable surface area when adsorbed onto the fibres, which leads to the discrepancy between values.

3.3. Sulfonated hypercrosslinked polymer-based supercapacitor performance

We varied the concentration of SHCP in the EPD suspension containing a fixed Na-CMC binder concentration of 0.45 g/L to investigate the impact on the specific capacitance (C_s) of SHCP coated carbon fibre electrodes. Initial electrochemical properties were measured for SCs containing solely liquid electrolyte, i.e. monofunctional SCs. Average capacitance increased with increasing SHCP concentration up to 3 g/L (Fig. 3a). The variation between repeated measurements may be a result of weak binding of the SHCP to the carbon fibres, causing the particles to detach during handling when immersed in the liquid electrolyte. To confirm the statistical difference between each concentration, a Student's t-test was performed. Each set of data was compared to the measured specific capacitances from devices produced via EPD from the 3 g/L suspension. The *t*-test confirmed a statistically significant capacitance increase until an SHCP concentration of 3 g/L ($t < 0.02$) but no significant difference between 3 and 4 g/L suspensions ($t > 0.99$). SC devices comprising electrodes produced from 10 g/L EPD suspensions were also investigated but again showed no improvement over the 3 and 4 g/L derived electrodes (Fig. S5). SHCP does not display long-range electron pair conjugation due to the formation of methylene crosslinks between aromatic rings and is therefore not an electron conductor. Surprisingly, however, we measured the capacitances of monofunctional SCs in the same range as those reported for graphene coated carbon fibres ($C_s = 1.5 \pm 0.2$ F/g [21]) but much lower than for single walled

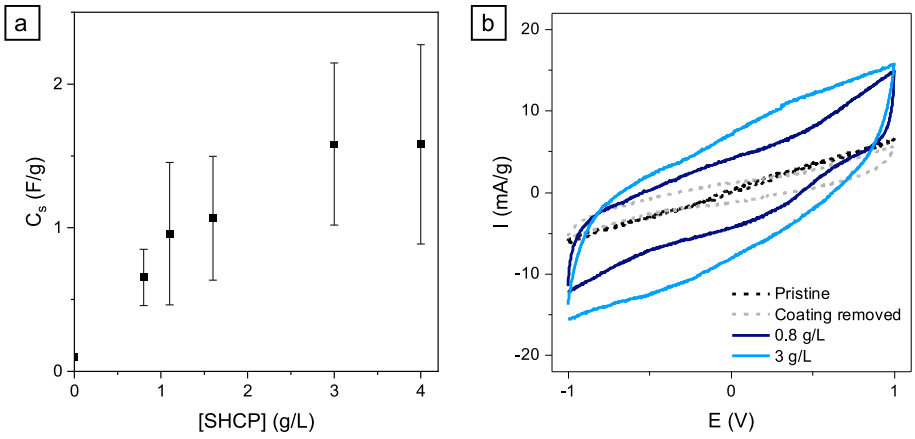

Fig. 3. A) Specific capacitance as a function of SHCP concentration in the EPD bath used for production of carbon fibre electrodes for monofunctional SCs, i.e. containing a liquid electrolyte. b) CV curves of monofunctional SCs comprising electrodes EPD coated from 0.8 g/L and 3 g/L SHCP suspensions. Devices containing pristine fibres and fibres after coating removal (initially EP deposited from a 4 g/L suspension) are also shown.

carbon nanotube (SWCNT) coated carbon fibres (up to $C_s = 16.6$ F/g for Supergrowth SWCNT coated carbon fibres [35]).

The shape of CV curves of monofunctional SCs, containing only liquid electrolyte (Fig. 3b), are close to that of ideal theoretical SCs. The curves are, however, slightly tilted due to the high resistance of the system as carbon fibres are three orders of magnitude less electronically conductive than aluminium, which is conventionally used as current collector for SCs. To confirm that the capacitance was due to the presence of the polymer, we retested the performance of the fibres after removing the SHCP coating, which was EP deposited from a 4 g/L suspension. We removed the coating by sonicating the carbon fibres for 30 min in water. The fibres were then rinsed with water and the process repeated twice. SEM images of the sonicated fibres confirmed the almost complete removal of SHCP from the fibre's surfaces (Fig. S6). The resulting carbon fibres were then assembled in a monofunctional SC, the C_s of which was 0.2 F/g, as compared to $C_s = 1.6 \pm 0.7$ F/g for coated fibres and $C_s = 0.1$ F/g for pristine carbon fibres. The remaining capacitance was likely due to some residual SHCP attached to the carbon fibres.

Structural composite supercapacitors, i.e. multifunctional SCs, were assembled with SHCP coated carbon fibre electrodes using optimised suspensions of 3 g/L of SHCP and 0.45 g/L of binder. The binder concentration was selected as it did not have a significant influence on the electrochemical performance of the assembled structural SCs (Fig. S7). The active portion of the assembled structural SC had an area of 9.5–11.8 cm^2, depending on the width of the spread carbon fibre tow electrode. Structural SCs weighed 218–271 mg, accounting for 55% of the total weight of the devices when considering the surplus separator and carbon fibre connectors. The fibre volume fraction (FVF) in the active component of the structural SCs was 21.2 ± 2.2%. This FVF is close to graphene based structural SC devices made without separator using a similar assembly procedure [21]. The FVF is low when compared to typical structural carbon fibre composites. The low FVF can be explained by two factors: i) the presence of the separator limits the achievable FVF in this layup, ii) the infusion process of the structural electrolyte into the carbon fibre preform is not common practice and should not be compared to conventional composite preparation processes, which reach around 60 vol% of carbon fibres [36].

Assembled structural SCs showed significantly improved reproducibility regarding C_s as compared to monofunctional SCs containing just liquid electrolyte. When the structural electrolyte is cured it prevents significant detachment of the SHCP particles from the carbon fibres, leading to greatly reduced variation between equivalent SCs. Structural SCs assembled with two electrodes had a specific capacity of 1.2 ± 0.2 F/g, in the range of previously measured values for structural SCs comprising graphene coated carbon fibre electrodes [21] but two orders of magnitude higher than multifunctional SWCNT infiltrated carbon fibre SCs ($C_s = 34.9$ mF/g). When assembling supercapacitors with eight electrodes (i.e. four of each polarity), the measured C_s reached 1.5 ± 0.1 F/g. No significant difference was found between the electrochemical behaviour of the SCs in liquid (Fig. 3b) or structural electrolyte (Fig. 4a); the measured capacitances are in the same range and the CV curves remained similar at the studied scan rates. The CV curves at increasing scan rates for a structural SC device made using electrodes prepared from 3 g/L SHCP suspension deviated from the ideal rectangular shape, due to reduced ion mobility and high internal resistance (Fig. 4b). The device possessed the highest specific capacitance of 1.45 F/g at 5 mV/s and decreased to around 0.19 F/g at a scan rate of 100 mV/s. The current peaks around 1 V and – 1 V were attributed to the beginning of water splitting at the electrodes' surface. A rate-dependent charge-discharge test was also performed from 0.5 to 4 mA/g and stable discharge phenomena were observed until 4 mA/g (Fig. 4c). The device displayed

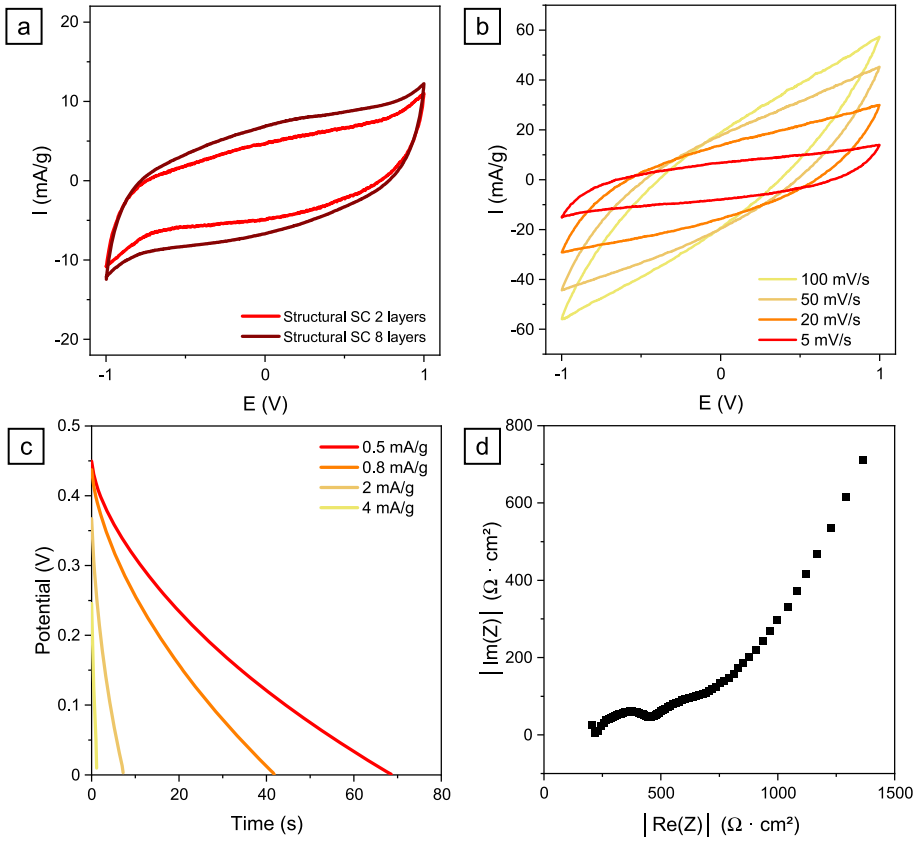

Fig. 4. Electrochemical performance of multifunctional SCs comprising SHCP coated carbon fibre electrodes and crosslinked PEGDGE containing 10 wt% EMIM BF_4 as structural electrolyte. a) CV curves of 2 or 8 electrode layer devices, b) CV curves of a 2-layer structural SC at various scan rates. c) rate dependent discharge tests for a two-layer structural SC. d) Characteristic Nyquist plot of a structural supercapacitor at room temperature and relative humidity (~33%).

a coulombic efficiency of ~97% at a current charge-discharge density of 0.4 mA/g (charge-discharge curve shown in Fig. S8).

We used electrochemical impedance spectroscopy to produce a Nyquist plot from which we estimated the equivalent series resistance (ESR) of structural SCs to be 0.65 ± 0.21 kΩ cm^2 (Fig. 4d). The ESR was significantly lower than other devices containing similar structural electrolyte systems [11,13] yet higher than that of supercapacitors using electrolytes with higher ionic conductivity [37]. At least two time constants can be seen in the Nyquist plot, as suggested by the appearance of at least two semi-circles. The semi-circle at higher frequency can be attributed to electrolyte resistances, i.e. resistance encountered as ions move through the structural electrolyte. The second semi-circle may be attributed to diffuse layer resistance, which is harder to define in this case as it arises due to various factors, such as ion size and charge, electrolyte properties, and electrode material composition [33]. Further sources of resistance may include poor contact between the carbon fibres used as current collector and aluminium tabs or poor adhesion of SHCP particles to carbon fibres. PEGDGE-based electrolytes, as used here, typically have an ionic conductivity of $\sigma \approx 10^{-5}$ S/cm [10] as compared to $\sigma \approx 10^{-2}$ S/cm for standard electrolytes [38,39]. This lower ionic conductivity inevitably results in high internal resistance in the assembled structural SCs. We can, in part, mitigate problems associated with poor ionic conductivity by producing thinner composite structural SCs. However, lowering specimen thickness at a fixed FVF will lower the structural SC's flexural modulus. Structural electrolytes with higher ionic conductivity, such as bicontinuous electrolytes, were reported but their preparation is significantly more labour intensive [37].

We assessed the capacitance retention of the assembled structural SCs as a function of cycle number using CV (Fig. 5a). When using high voltage (4 V) capacitance faded quickly, reaching 50% of the initial capacitance after only 20 cycles. The capacitance fading is likely due to water splitting at the electrodes as the structural SCs were not protected from ambient moisture, degrading the electrode-electrolyte interface by production of H_2 and O_2, reducing the interfacial area, thus lowering the capacitance. When cycling up to 1 V capacitance also faded, reaching 50% of the initial capacitance after 483 cycles at 50 mV/s and 507 cycles at 20 mV/s. When cycling between −0.5 V and 0.5 V at a temperature of 21 °C and humidity of around 58% RH the capacitance remained at 96% of the initial capacitance even after 3500 cycles, demonstrating stability in this voltage range (Fig. S9). We also cycled two devices 1 year after manufacture at a rate of 6.6 mV/s over a voltage range of −1 to 1 V for 10 days and found no significant loss of electrochemical performance (Fig. S10). Small deviations from the general trend of the curves derive from the calculation method, which only considered two points per cycle. The larger variations are attributed to a change of temperature and/or humidity in the laboratory during the measurements (Fig. S9). It is important to note that the structural SCs had poor performances when tested in inert dry atmosphere. When taken out of the glovebox in a sealed pouch and tested, the capacitance of the assembled structural SCs was in the range of pristine carbon fibres (Fig. S10). This observation indicates that moisture plays a major role in the energy storage mechanism of the SHCP coated carbon fibre electrodes.

We investigated the impact of relative humidity (RH) on the electrochemical performance of structural SCs; increasing the RH resulted in increased capacity of SHCP-based devices (Fig. 5b). Characteristic Nyquist plots are shown in Fig. S11. The ionic conductivity of SHCPs increased with increasing RH, in good agreement with literature for the proton conductivity of SHCPs formed by post-polymerisation sulfonation of hypercrosslinked biphenyl (S-POP-BP), which increases from $9{\cdot}10^{-5}$ S/cm at 40% RH to $1{\cdot}10^{-2}$ S/cm at 95% RH [40]. In a SC, the energy storage mechanism requires charge mobility from the surface of the electrodes to the current collector. Increased moisture content led to increased H^+ mobility in the SHCP particles attached to the carbon fibres.

The energy and power densities of structural SCs were calculated using Eq. (3) and Eq. (4), respectively, to be $E = 39 \pm 6$ mWh/kg and $P = 15 \pm 4$ W/kg for an operating voltage of 0.5 V. Both were calculated from the data acquired for multifunctional structural SCs tested at room temperature and ambient RH. The capacity used for the calculation was extracted from CV between – 1 V and 1 V at 5 mV/s and the ESR value from EIS. These values greatly exceed those of similar devices reported elsewhere (juxtaposed in Table 1). Although higher energy and power densities have been reported elsewhere [37], comparison is discouraged as evidence of mechanical integrity was not provided. Therein, the authors tested various layups combining carbon aerogel (CAG) coated carbon fibre electrodes partially filled with structural electrolyte and then soaked in liquid electrolyte to fill the remaining void space of the electrodes [37]. The average characteristics of our SHCP-based structural composite SCs assembled in a PEGDGE-based structural electrolyte are summarised in Table 2. We calculated the energy and power density values for an operating voltage of 0.5 V as it was not possible to cycle the SCs without capacity loss at higher voltages.

To assess mechanical properties, we produced (example shown in Fig. S12) and tested (Fig. S13) multifunctional SHCP-based structural SCs. The average tensile strength of the structural SC demonstrators was 495 ± 42 MPa and the Young's modulus 49 ± 4 GPa, in good agreement with our previous work on devices consisting of graphene coated carbon fibres in the same electrolyte system [21] albeit with a lower FVF. We also produced monofunctional composites comprising bare carbon fibre reinforced structural electrolyte, which had similar mechanical properties and FVF (23.4%), showing that SHCP deposition is neither detrimental nor beneficial for the mechanical performance. Mechanical

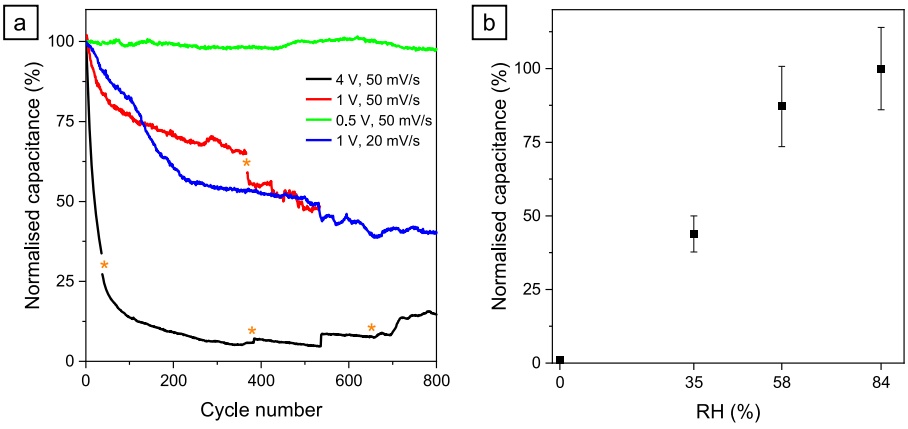

Fig. 5. A) Normalised capacitance of structural supercapacitors a) as a function of cycle number for various testing conditions (* indicate a pause in the measurement) and b) as a function of RH. The capacitance was normalised to that of devices tested at an 84% RH.

Table 1
Comparison of the energy and power densities of reported structural composite SCs normalised to the mass of the electrodes and of tensile properties of structural SCs.

Electrode	*E* (mWh/kg)	*P* (W/kg)	σ (MPa)	*E* (GPa)	Ref.
Chemically activated carbon fibres[a]	1.4	2.7	b	b	[41]
CAG coated carbon fibres[a]	0.8	0.03	c	c	[11]
CAG coated carbon fibres[a]	93[d]	5.2[d]	110[b]	33	[12]
SWCNT infiltrated carbon fibres[a]	1.6	0.19	245 ± 12	17 ± 1	[33]
Graphene coated carbon fibres[a]	2.9	1.14	294 ± 9	24 ± 2	[13]
Graphene coated carbon fibres	16.9	5.2	350 ± 100	26 ± 3	[21]
SHCP coated carbon fibres	39.0	15.4	495 ± 42	49 ± 4	This work
Bare carbon fibres	–	–	580 ± 54	54 ± 2	This work

[a] Devices comprising woven carbon fibre.
[b] Compression properties were reported.
[c] In-plane shear properties were determined.
[d] Electrical properties were tested on small scale devices in a Swagelok cell.

Table 2
Summary of the properties of multifunctional SHCP-based structural composite supercapacitors.

Surface (cm^2)	Thickness (μm)	C_s (F/g)	ESR (kΩ·cm^2)	E (mWh/kg)	P (W/kg)	FVF (%)
10.4 ± 0.9	225 ± 34	1.2 ± 0.2	0.65 ± 0.21	39 ± 6	15 ± 4	21.2 ± 2.2

properties of our multifunctional SCs are compared to other structural composite supercapacitors in Table 1.

Potential mass savings are assessed by calculating the multifunctional efficiency [42] η_{MF} of SHCP-based structural composite SCs, which is defined as: $\eta_{MF} = \frac{E_{MF}}{E_{Mono}} + \frac{\Gamma_{MF}}{\Gamma_{Mono}}$, where E is the Young's modulus and Γ the energy density of the mono- or multifunctional material. When comparing our mono- and multifunctional SCs $\eta_{MF} = 1.66$. However, we believe such comparisons are unfair representations and state-of-the-art monofunctional materials/devices should be used for this assessment. In this case, we estimate η_{MF} would be closer to 0.4, highlighting the need for further improvements in energy density, increased FVF of multifunctional composites and mechanical properties of the structural electrolyte: the weakest component of structural SCs.

4. Conclusion

We describe a new class of porous polymer electrode material for structural supercapacitors, achieving energy and power densities of 39 mWh/kg and 15 W/kg, respectively, among the highest values reported. By employing highly sulfonated hypercrosslinked polymers, these porous networks were successfully suspended in water for subsequent electrophoretic deposition. In addition to desirable surface area, the acidic sulfonic acid moieties imparted ionic conductivity to the electrode materials in the presence of sufficient moisture. Structural composite supercapacitors were assembled with 21 vol% SHCP decorated carbon fibres as electrodes and possessed specific capacitance up to 1.5 F/g when using a structural electrolyte saturated with moisture at 35% RH. RH strongly affected the capacitance, indicating that adsorbed water is key for the ion conduction mechanism of SHCP particles. These structural composite supercapacitors possessed a tensile strength and Young's modulus of 495 MPa and 49 GPa, respectively. By successful implementation of HCPs as electrode material, a broad array of new structural SC design options are unveiled, including more water tolerant materials.

Author statement

OH: experimental design, experiments, data collection and analysis, manuscript drafting and revision. NT, LMRG, EG, ABl, AM: experiments, data collection and testing. RTW: data collection and analysis, conceptualisation, manuscript writing and revision and supervision. AB: data collection and analysis, conceptualisation, manuscript writing and revision, supervision and funding acquisition.

Declaration of competing interest

The authors declare that they have no known competing financial interests or personal relationships that could have appeared to influence the work reported in this paper.

Data availability

Data will be made available on request.

Acknowledgements

This research was performed in the framework of HyFiSyn project funded by the European Union's Horizon 2020 research and innovation programme under the Marie Skłodowska-Curie grant agreement No 765881 and funded OH. LMRG is grateful for the financial support of Erasmus+. We acknowledge the help of Amy Ho with mechanical tests, Qixiang Jiang for the long term cyclovoltammetry and Maria Waldl (all Univie) for helping manage big electrochemical data sets. We also thank Derrick Fam (A*STAR, Singapore) for fruitful discussions regarding EIS.

Appendix A. Supplementary data

Supplementary data to this article can be found online at https://doi.org/10.1016/j.compscitech.2023.110152.

References

[1] W. Johannisson, D. Zenkert, G. Lindbergh, Model of a structural battery and its potential for system level mass savings, Multifunct. Mater. 2 (3) (2019), 035002, https://doi.org/10.1088/2399-7532/ab3bdd.
[2] J. Zhang, J. Yan, Y. Zhao, Q. Zhou, Y. Ma, Y. Zi, A. Zhou, S. Lin, L. Liao, X. Hu, H. Bi, High-strength and machinable load-bearing integrated electrochemical capacitors based on polymeric solid electrolyte, Nat. Commun. 14 (2023) 64, https://doi.org/10.1038/s41467-022-35737-w.
[3] E.S. Greenhalgh, S. Nguyen, M. Valkova, N. Shirshova, M.S.P. Shaffer, A.R. J. Kucernak, A critical review of structural supercapacitors and outlook on future research challenges, Compos. Sci. Technol. 235 (2023), 109968, https://doi.org/10.1016/j.compscitech.2023.109968.
[4] J.T. South, R.H. Carter, J.F. Snyder, C.D. Hilton, D.J. O'Brien, E.D. Wetzel, Multifunctional power-generating and energy-storing structural composites for U. S. Army applications, Mater. Res. Soc. Symp. Proc. 851 (2004) 269–280, https://doi.org/10.1557/PROC-851-NN4.6.
[5] X. Luo, D.D.L. Chung, Carbon-fiber/polymer-matrix composites as capacitors, Compos. Sci. Technol. 61 (6) (2001) 885–888, https://doi.org/10.1016/S0266-3538(00)00166-4.
[6] J.F. Snyder, E.L. Wong, C.W. Hubbard, Evaluation of commercially available carbon fibers, fabrics, and papers for potential use in multifunctional energy storage applications, J. Electrochem. Soc. 156 (2009) A215, https://doi.org/10.1149/1.3065070.
[7] J. Zhao, A.F. Burke, Electrochemical capacitors: materials, technologies and performance, Energy Storage Mater. 36 (2021) 31–55, https://doi.org/10.1016/j.ensm.2020.12.013.
[8] A.G. Pandolfo, A.F. Hollenkamp, Carbon properties and their role in supercapacitors, J. Power Sources 157 (1) (2006) 11–27, https://doi.org/10.1016/j.jpowsour.2006.02.065.
[9] H. Qian, H. Diao, N. Shirshova, E.S. Greenhalgh, J.G.H. Steinke, M.S.P. Shaffer, A. Bismarck, Activation of structural carbon fibres for potential applications in multifunctional structural supercapacitors, J. Colloid Interface Sci. 395 (2013) 241–248, https://doi.org/10.1016/j.jcis.2012.12.015.

[10] N. Shirshova, H. Qian, M. Houllé, J.H.G. Steinke, A.R.J. Kucernak, Q.P.V. Fontana, E.S. Greenhalgh, A. Bismarck, M.S.P. Shaffer, Multifunctional structural energy storage composite supercapacitors, Faraday Discuss 172 (2014) 81–103, https://doi.org/10.1039/C4FD00055B.
[11] H. Qian, A.R. Kucernak, E.S. Greenhalgh, A. Bismarck, M.S.P. Shaffer, Multifunctional structural supercapacitor composites based on carbon aerogel modified high performance carbon fiber fabric, ACS Appl. Mater. Interfaces 5 (13) (2013) 6113–6122, https://doi.org/10.1021/am400947j.
[12] M.F. Pernice, G. Qi, E. Senokos, D.B. Anthony, S. Nguyen, M. Valkova, E. S. Greenhalgh, M.S.P. Shaffer, A.R.J. Kucernak, Mechanical, electrochemical and multifunctional performance of a CFRP/carbon aerogel structural supercapacitor and its corresponding monofunctional equivalents, Multifunct. Mater. 5 (2022), 025002, https://doi.org/10.1088/2399-7532/ac65c8.
[13] X.F. Sánchez-Romate, A.D. Bosque, J. Artigas-Arnaudas, B.K. Muñoz, M. Sánchez, A. Ureña, A proof of concept of a structural supercapacitor made of graphene coated woven carbon fibers: EIS study and mechanical performance, Electrochim. Acta 370 (2021), 137746, https://doi.org/10.1016/j.electacta.2021.137746.
[14] B.K. Deka, A. Hazarika, S. Lee, D.Y. Kim, Y.-B. Park, H.W. Park, Triboelectric-nanogenerator-integrated structural supercapacitor based on highly active P-doped branched Cu–Mn selenide nanowires for efficient energy harvesting and storage, Nano Energy 73 (2020), 104754, https://doi.org/10.1016/j.nanoen.2020.104754.
[15] B.K. Deka, A. Hazarika, M.-J. Kwak, D.C. Kim, A.P. Jaiswal, H.G. Lee, J. Seo, C. Jeong, J.-H. Jang, Y.-B. Park, H.W. Park, Triboelectric nanogenerator-integrated structural supercapacitor with in situ MXene-dispersed N-doped Zn–Cu selenide nanostructured woven carbon fiber for energy harvesting and storage, Energy Storage Mater. 43 (2021) 402–410, https://doi.org/10.1016/j.ensm.2021.09.027.
[16] B.K. Deka, A. Hazarika, O. Kwon, D. Kim, Y.-B. Park, H.W. Park, Multifunctional enhancement of woven carbon fiber/ZnO nanotube-based structural supercapacitor and polyester resin-domain solid-polymer electrolytes, Chem. Eng. J. 325 (2017) 672–680, https://doi.org/10.1016/j.cej.2017.05.093.
[17] H.C. Hamaker, Formation of a deposit by electrophoresis, Trans. Faraday Soc. 35 (1940) 279–287, https://doi.org/10.1039/TF9403500279.
[18] N.A. Kyerematen, T.M. Dinh, D. Pech, Electrophoretic deposition of Li4Ti5O12 nanoparticles with a novel additive for Li-ion microbatteries, RSC Adv. 5 (2015) 61502–61507, https://doi.org/10.1039/C5RA11039D.
[19] M. Shrestha, I. Amatya, K. Wang, B. Zheng, Z. Gu, Q.H. Fan, Electrophoretic deposition of activated carbon YP-50 with ethyl cellulose binders for supercapacitor electrodes, J. Energy Storage 13 (2017) 206–210, https://doi.org/10.1016/j.est.2017.07.015.
[20] C.C. Lalau, C.T.J. Low, Electrophoretic deposition for lithium-ion battery electrode manufacture, Batter. Supercaps. 2 (6) (2019) 551–559, https://doi.org/10.1002/batt.201900017.
[21] O. Hubert, N. Todorovic, A. Bismarck, Towards separator-free structural composite supercapacitors, Compos. Sci. Technol. 217 (2022), 109126, https://doi.org/10.1016/j.compscitech.2021.109126.
[22] L. Tan, B. Tan, Hypercrosslinked porous polymer materials: design, synthesis, and applications, Chem. Soc. Rev. 46 (2017) 3322–3356, https://doi.org/10.1039/C6CS00851H.
[23] B. Li, R. Gong, W. Wang, X. Huang, W. Zhang, H. Li, C. Hu, B. Tan, A new strategy to microporous polymers: knitting rigid aromatic building blocks by external cross-linker, Macromolecules 44 (8) (2011) 2410–2414, https://doi.org/10.1021/ma200630s.
[24] L. Prince, P. Guggenberger, E. Santini, F. Kleitz, R.T. Woodward, Metal-Free hyper-cross-linked polymers from benzyl methyl ethers: a route to polymerization catalyst recycling, Macromolecules 54 (19) (2021) 9217–9222, https://doi.org/10.1021/acs.macromol.1c01332.
[25] A. Stephenson, B. Li, L. Chen, R. Clowes, M.E. Briggs, A.I. Cooper, Efficient separation of propane and propene by a hypercrosslinked polymer doped with Ag (I), J. Mater. Chem. A. 7 (2019) 25521–25525, https://doi.org/10.1039/C9TA07510K.
[26] R.T. Woodward, M. Kessler, S. Lima, R. Rinaldi, Hypercrosslinked microporous polymer sorbents for the efficient recycling of a soluble acid catalyst in cellulose hydrolysis, Green Chem. 20 (2018) 2374–2381, https://doi.org/10.1039/C8GC00573G.
[27] J.-Y. Lee, C.D. Wood, D. Bradshaw, M.J. Rosseinsky, A.I. Cooper, Hydrogen adsorption in microporous hypercrosslinked polymers, Chem. Commun. (2006) 2670–2672, https://doi.org/10.1039/B604625H.
[28] Y. Gu, S.U. Son, T. Li, B. Tan, Low-cost hypercrosslinked polymers by direct knitting strategy for catalytic applications, Adv. Funct. Mater. 31 (2021), 2008265, https://doi.org/10.1002/adfm.202008265.
[29] G.E.M. Schukraft, R.T. Woodward, S. Kumar, M. Sachs, S. Eslava, C. Petit, Hypercrosslinked polymers as a photocatalytic platform for visible-light-driven CO2 photoreduction using H2O, ChemSusChem 14 (7) (2021) 1720–1727, https://doi.org/10.1002/cssc.202002824.
[30] R. Vinodh, C.V.V.M. Gopi, V.G.R. Kummara, R. Atchudan, T. Ahamad, S. Sambasivam, M. Yi, I.M. Obaidat, H.-J. Kim, A review on porous carbon electrode material derived from hypercross-linked polymers for supercapacitor applications, J. Energy Storage 32 (2020), 101831, https://doi.org/10.1016/j.est.2020.101831.
[31] V. Sharma, A. Sahoo, Y. Sharma, P. Mohanty, Synthesis of nanoporous hypercrosslinked polyaniline (HCPANI) for gas sorption and electrochemical supercapacitor applications, RSC Adv. 5 (2015) 45749–45754, https://doi.org/10.1039/C5RA03016A.
[32] A. Blocher, F. Mayer, P. Schweng, T.M. Tikovits, N. Yousefi, R.T. Woodward, One-pot route to fine-tuned hypercrosslinked polymer solid acid catalysts, Mater. Adv. 3 (2022) 6335–6342, https://doi.org/10.1039/D2MA00379A.
[33] B.-A. Mei, O. Munteshari, J. Lau, B. Dunn, L. Pilon, Physical interpretations of nyquist plots for EDLC electrodes and devices, J. Phys. Chem. C 122 (1) (2018) 194–206, https://doi.org/10.1021/acs.jpcc.7b10582.
[34] R.T. Woodward, The design of hypercrosslinked polymers from benzyl ether self-condensing compounds and external crosslinkers, Chem. Commun. 56 (2020) 4938–4941, https://doi.org/10.1039/D0CC01002B.
[35] E. Senokos, D.B. Anthony, N. Rubio, M.C. Ribadeneyra, E.S. Greenhalgh, M.S. P. Shaffer, Robust single-walled carbon nanotube-infiltrated carbon fiber electrodes for structural supercapacitors: from reductive dissolution to high performance devices, Adv. Funct. Mater. (2023), 2212697, https://doi.org/10.1002/adfm.202212697.
[36] L.G. Stringer, Optimization of the wet lay-up/vacuum bag process for the fabrication of carbon fibre epoxy composites with high fibre fraction and low void content, Compos 20 (5) (1989) 441–452, https://doi.org/10.1016/0010-4361(89)90213-9.
[37] G. Qi, S. Nguyen, D.B. Anthony, A.R.J. Kucernak, M.S.P. Shaffer, E.S. Greenhalgh, The influence of fabrication parameters on the electrochemical performance of multifunctional structural supercapacitors, Multifunct. Mater. 4 (2021), 034001, https://doi.org/10.1088/2399-7532/ac1ea6.
[38] H.P. Chen, J.W. Fergus, B.Z. Jang, The effect of ethylene carbonate and salt concentration on the conductivity of propylene Carbonate|Lithium perchlorate electrolytes, J. Electrochem. Soc. 147 (2000) 399, https://doi.org/10.1149/1.1393209.
[39] E.Y. Tyunina, V.N. Afanasiev, M.D. Chekunova, Electroconductivity of tetraethylammonium tetrafluoroborate in propylene carbonate at various temperatures, J. Chem. Eng. Data 56 (7) (2011) 3222–3226, https://doi.org/10.1021/je200309v.
[40] Z. Li, Y. Yao, D. Wang, M.M. Hasan, A. Suwansoontorn, H. Li, G. Du, Z. Liu, Y. Nagao, Simple and universal synthesis of sulfonated porous organic polymers with high proton conductivity, Mater. Chem. Front. 4 (2020) 2399, https://doi.org/10.1039/D0QM00276C, 2345.
[41] N. Shirshova, H. Qian, M.S.P. Shaffer, J.H.G. Steinke, E.S. Greenhalgh, P.T. Curtis, A. Kucernak, A. Bismarck, Structural composite supercapacitors, Compos. -A: Appl. Sci. Manuf. 46 (2013) 96–107, https://doi.org/10.1016/j.compositesa.2012.10.007.
[42] D.J. O'Brien, D.M. Baechle, E.D. Wetzel, Design and performance of multifunctional structural composite capacitors, J. Compos. Mater. 45 (2011) 2797–2809, https://doi.org/10.1177/0021998311412207.